Magnetically-programmed instability-driven pattern transformations in soft materials

Magnetically-programmed instability-driven pattern transformations in soft materials

Nitesh Arora[1], Vincent Chen[2,3], Andrei Cherkasov[4], Yuhai Xiang[5], Abigail Juhl[2], Philip Buskohl[2], Stephan Rudykh[1,4,*]

[1] *Department of Mechanical Engineering, University of Wisconsin–Madison, Madison, WI, USA*

[2] *Air Force Research Laboratory, Wright-Patterson AFB, Ohio, USA*

[3] *UES, Inc., Dayton, Ohio, USA*

[4] *School of Mathematical and Statistical Sciences, University of Galway, Ireland*

[5] *Department of Chemical Engineering and Materials Science, University of Minnesota, Minneapolis, USA*

Abstract

We introduce a class of transformable materials with magnetic defect-defined switchable configurations. The soft material can be magnetically-programmed to transform into various encoded patterns utilizing the rich interplay of magnetic interactions and instability phenomenon. The strategy allows us to break the limit of admissible configurations of the instability-induced patterns that dictate the post-transformation behavior. We experimentally realize the phenomenon in a material system consisting of periodically distributed magnetic inclusions in a soft matrix. The programmable magnetic interactions between the inclusions act as smart defects redirecting the material transformations to targeted geometric configurations. Moreover, we systematically investigate the role of magnetic spacing and field strength to map the transition between mechanically-dominant and magnetics-dominant instability patterns. Lastly, we showcase the idea of reconfigurable material design by embedding binary information in magnetic form, which can be read out through the unique repositioning of inclusions via the applied mechanical deformation.

*Corresponding author: Stephan Rudykh (rudykh@wisc.edu)

1 Introduction

The ability to reconfigure the microstructure of architected materials forms the basis for designing material-based systems with switchable functionalities [1–5]. Moreover, microstructural transformations equip the materials with shape-shifting and morphing capabilities [6–8], which are critical for various applications, including soft robotics [9] and deployable devices [10]. *Soft* deformable architectures represent an ideal platform for the design of such tunable materials, thanks to their morphing capability in response to external stimuli [11–16]. Moreover, elastic instability phenomenon observed in these materials has been identified as a powerful tool to trigger sudden but controlled and reversible microstructural transformations [17–19]. This approach has been employed for designing materials with tunable Poisson's ratio [20], phononic and photonic switches [21, 22], and color displays [23]. Notably, in all these applications, the post-instability behavior of the material is uniquely determined by its buckling characteristics.

Instability-driven microstructural transformations are studied in various architected materials. For example, periodic lattices exhibit mechanical instability by sequential buckling of inner elements [24, 25]. In soft porous architectures, the voids collapse in a cooperative manner leading to an internal reconfiguration of the microstructure [17]. Moreover, multi-phase architected composites [26] can develop a rich variety of post-buckling patterns [27–29]. In all these architectures, the characteristics of the buckling patterns – periodicity and amplitude – are defined by the initial microstructure patterning and mechanical properties of constituent materials. However, the geometry of admissible patterns is highly limited when the instability development is solely governed via the mechanical stress-fields; in general, the patterns are spatially homogeneous and periodic. This also restricts their employability in challenging applications such as soft robotics and actuation [30, 31], prosthetics [32], wearable technologies [33–36], and mechanical computers [37, 38], which demand local control on the reconfigurability of the architected materials.

Here, we present how the magneto-mechanical coupling in soft architected materials can be exploited to break the limit of admissible instability-induced patterns. We consider soft particulate composites with periodically distributed stiff magnetic inclusions in a soft matrix (Fig. 1a). An individual magnetic inclusion has one of either magnetic polarization: towards the positive or negative $x-$direction (Fig. 1b). We first compare the distinct microstructure evolution in composites with magnetically active and inactive inclusions, via applied deformation. We then investigate the different classes of buckling patterns, based on the competition between the mechanical and magnetic interactions among the inclusions. Through our experiments and simulations, we show that in the magnetically-dominated regime, the reconfiguration of inclusions is solely guided by

the local magnetic forces, which can be pre-programmed. Finally, we show that the soft composites can develop arbitrary binary (two-level) instability patterns, based on the encoded magnetic polarity-arrangement. We showcase the diversity of the admissible structural transformations through a series of information embedding demonstrations, including alphabet shape matching and Morse code.

2 Results and discussion

2.1 Mechanical and magnetic instability patterns

To understand the influence of using magnetically active inclusions in the particulate composite, we start with comparing its response to that of the *purely mechanical* counterpart (with magnetically inactive inclusions). We fabricated the magnetic particulate composites by setting neodymium magnets (B422, K&J Magnetics) in a silicone matrix (Mold Max 10T, Smooth-On, shear modulus $G_m = 0.1$ MPa). Geometrically, the composite is described using the spacing ratio $\xi = a/w$; w is the width of the primitive unit cell (bounded by dashed lines in Fig. 1a) and a is the side of the rigid square inclusion. The magnets have a square cross-section with side $a = 3.175$ mm and out-of-plane thickness $d = 6.35$ mm. In experiments, we consider the specimen with height $h = 51.2$ mm consisting of $N = 18$ unit cells (additional details on specimen preparation are provided in Supplementary Sec. S1). The compression tests are performed using a high torque stepper motor-based linear actuator. The specimens are compressed quasistatically along the $x-$direction. To prevent out-of-plane deformation, the composite is placed between the transparent parallel-plate fixture to maintain plane-strain conditions (for more details on the experimental setup, see Supplementary Sec. S2).

The simulations are performed using the finite element code (COMSOL Multiphysics 6.0). The soft matrix is modeled as nearly incompressible magnetically inactive neo-Hookean material, whereas the magnetic inclusions are considered to be rigid. With the development of instabilities, the composite breaks its initial periodicity and rigid inclusions can rearrange into new patterns. To capture these reconfigurations in our simulations, we model representative volume elements (RVEs) consisting of multiple unit cells. A detailed description of modeling, magnetic characterization, and instability analysis is provided in Supplementary Sec. S3.

As an illustrative example, we consider the magnetic composite in which the adjacent inclusions have opposite polarities. Physically, the magnets are placed in a fashion such that the adjacent magnets repel each other. Note that for a fair comparison, the mechanical particulate composite

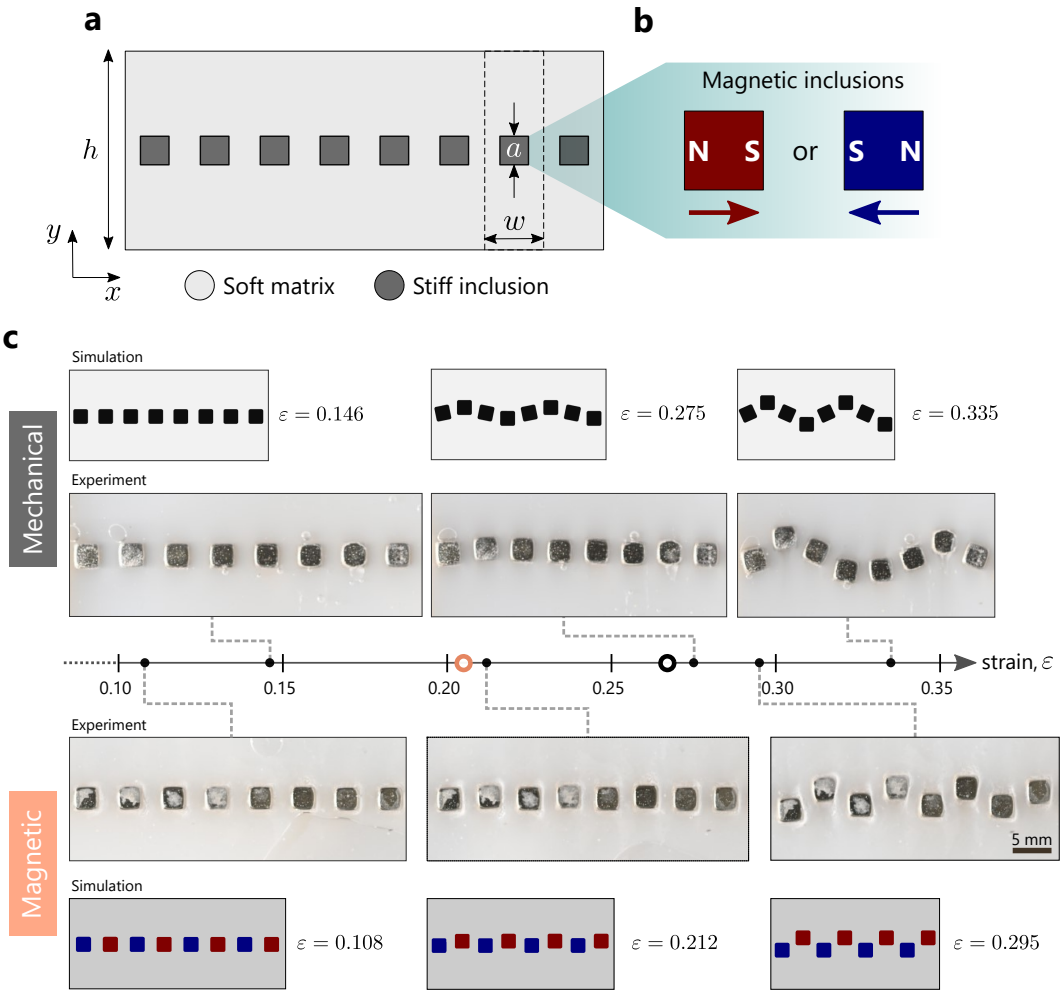

Figure 1: **Schematics and comparison of microstructure evolution in mechanical and magnetic composite with deformation.** **a**, Schematic of a periodic particulate composite with square rigid inclusions. The primitive unit cell is bounded by dashed lines. **b**, The square inclusion has either of the two orientations of magnetic polarity: either parallel or anti-parallel to the x-axis. **c**, Experimental and simulation images of mechanical (top) and magnetic composite (bottom) at different levels of compressive strain, ε. The orange hollow circle on the strain scale marks the experimental critical strain value for the magnetic composite, whereas the black hollow circle marks it for the mechanical composite. The results are shown for the composites with spacing ratio $\xi = a/w = 0.5$.

is prepared using demagnetized magnets. The inclusions are periodically placed with a distance $w = 6.35$ mm between their centers such that the spacing ratio is $\xi = 0.5$. In the simulation images of particulate composite, the magnetically inactive inclusions are shown in black color, whereas the magnets are shown in red and blue colors to represent positive and negative polarization, respectively.

Figure 1c shows the direct comparison between the evolution of microstructure in the mechanical and magnetic composites as the function of applied compressive strain ε. Both composites are subjected to large deformations, up to the compressive strain level of $\varepsilon = 0.35$. The mechanical composite maintains its initial periodicity of one unit cell up to the critical deformation level $\varepsilon_{cr} = 0.267$ (marked by a hollow black circle on the strain-scale in Fig. 1c). With the onset of instability, the soft composite breaks its initial periodicity ($N = 1$) and the rigid inclusions rearrange into the wavy pattern with a new periodicity of $N \approx 4$. On further deformation, the amplitude of the buckling pattern further accentuates, as can be seen in the deformation images at strains $\varepsilon = 0.275$ and $\varepsilon = 0.335$.

In the magnetic particulate composite, instability-induced microstructure reconfiguration takes place at a comparatively smaller deformation level, i.e., at $\varepsilon_{cr} = 0.205$ (marked by an orange hollow circle on the strain-scale). The decrease in critical strain can be attributed to the magnetic interaction between the inclusions. In particular, with the compression of the composite, the inclusions move closer to each other leading to a significant increase in the magnitude of repulsive forces among the oppositely polarized adjacent inclusions. As a result, in the post-instability regime, the inclusions arrange into two rows. The alternately-positioned inclusions, having positive magnetic polarity, shift cooperatively to constitute one of the rows. The remaining inclusions with negative polarity arrange together to form the other row of the buckling pattern (see deformation image of magnetic particulate composite at $\varepsilon = 0.295$). Clearly, this two-level pattern generated in the magnetic particulate composite is strikingly distinct from the wavy-pattern observed in its mechanical counterpart.

We note that our numerical predictions agree with the experimental results. In particular, for the mechanical composite (shown in Fig. 1c), the simulation predicts $\varepsilon_{cr} = 0.256$ and post-buckling periodicity $N = 4$; it is fairly close to the experimental ones: $\varepsilon_{cr} = 0.267$ and $N \approx 4.5$. For the magnetic composite, the simulation estimates $\varepsilon_{cr} = 0.210$ in comparison to $\varepsilon_{cr} = 0.205$ observed in experiments. Notably, the two-level pattern is accurately predicted in simulation as realized in experiments. Moreover, the reproducibility of this discrete pattern is verified experimentally in an additional specimen subjected to multiple loading cycles and we find that the pattern develops

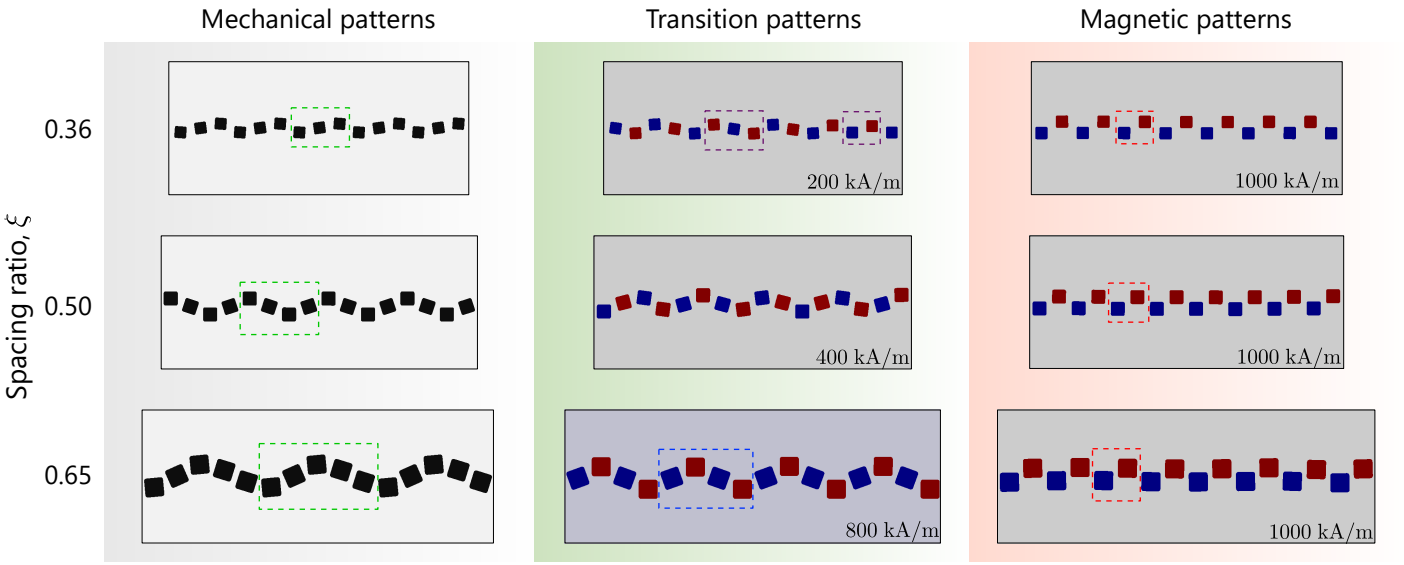

Figure 2: **Mechanical, transition, and magnetic instability patterns.** Simulation images of post-buckling patterns in the particulate composites with spacing ratio $\xi = 0.36$ (top row), $\xi = 0.50$ (center row), and $\xi = 0.65$ (bottom row). The results are shown for mechanical composites (left column), magnetic composites (middle and right column) with their magnetization values written at the bottom-right of each image.

consistently (more details in Supplementary Sec. S4).

2.2 Transition from mechanical to magnetic patterns

The results thus far illustrate that the magnetic interactions between the inclusions lead to a distinct instability pattern from the purely mechanical case. Next, to investigate the transition from mechanical to magnetic buckling pattern, we study how the instability characteristics change with the magnetic strength of the inclusions. We consider the composites with various spacing ratios, namely, $\xi = 0.36$, $\xi = 0.50$, and $\xi = 0.65$; the corresponding post-buckling simulation images are shown in Fig. 2 at the compressive strains of $\varepsilon = 0.4$, $\varepsilon = 0.3$, and $\varepsilon = 0.2$, respectively.

We observe that the mechanical composites develop wavy buckling patterns and their periodicity changes with the spacing ratio (left column in Fig. 2). In particular, the composite with $\xi = 0.36$, $\xi = 0.50$, and $\xi = 0.65$ rearrange into the patterns with increasing periodicity of $N = 3$, $N = 4$, and $N = 5$, respectively. The elements of periodic patterns in mechanical composites are marked by green-dashed rectangles.

Next, consider the magnetic composites with a large magnetization value of $M = 1000$ kA/m

(right column in Fig. 2). The magnets are placed such that they repel the adjacent ones (as also considered in Fig. 1c). In these composites, the inclusions rearrange to form the two-level buckling patterns with a periodicity of $N = 2$. This holds true regardless of the initial spacing ratio of the composites, which highlights that the formation of these patterns is dictated by the magnetic forces. The repeating elements are marked by the red-dashed rectangles in the right column.

Interestingly, for a certain range of magnetization values, the instability patterns neither resemble the mechanical patterns nor the two-level magnetic pattern. We classify these patterns as 'Transition patterns' (middle column in Fig. 2). For example, in the soft composite with $\xi = 0.36$ and $M = 200$ kA/m, we observe an irregular repetition of the base elements of size $N = 3$ and $N = 2$ (marked by the violet-dashed rectangles). Moreover, in the composite with $\xi = 0.50$ and $M = 400$ kA/m, the inclusions rearrange aperiodically. It is worth noting that although the design parameters – geometric placement of the inclusions and their magnetic polarity arrangement – of these composites are *periodic*, they generate these *quasi-periodic* and *aperiodic* instability patterns. Exceptionally, the magnetic composite with $\xi = 0.65$ and $M = 800$ kA/m develops a strictly periodic wavy-pattern. In particular, the inclusions rearrange to give rise to a new a periodicity of $N = 4$, which lies in between of the corresponding mechanical ($N = 5$) and magnetic ($N = 2$) patterns. The repeating base element is marked by the blue-dashed rectangle. Note that the composites shown in Fig. 2 are a few of the representative examples. In Supplementary Fig. S10, we present the formation of buckling patterns at various magnetization values in composites with $\xi = 0.50$.

The instability development in these composites is led by two mechanisms: (i) the chain of inclusions behaves similar to a reinforced layer in a soft matrix (or a laminate) and drives the formation of periodic wavy-patterns [28]; and (ii) the inclusions rearrange vertically to 'relax' the increasing magnetic forces as they are frustrated horizontally with an increasing strain. Controlled by the particle magnetization (for a given initial geometric configuration), the composites can develop mechanical, magnetic, or transition patterns governed by the complex interplay of the mechanical and magnetic mechanisms.

Next, to comprehensively study the characteristics of the instability development in the magneto-mechanical particulate composite, we examine its bifurcation eigenmodes by performing the Bloch-Floquet analysis on its unit cell (shown in Fig. 3a). In particular, we first finitely deform the unit cell by applying the strain ε and then investigate the propagation of small amplitude elastic waves with wavenumber k by superimposing the Bloch-Floquet periodicity conditions. Through the analysis, we obtain the critical strain ε_{cr} and wavenumber k_{cr} (for more details on the analysis see

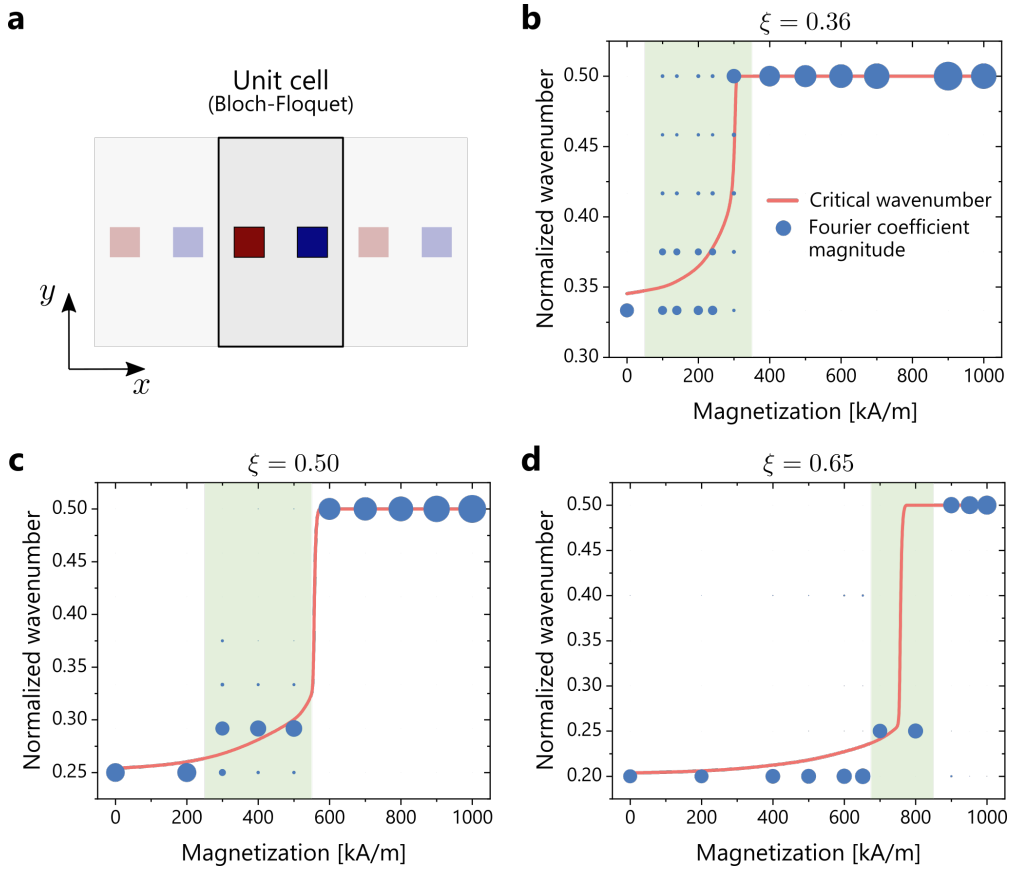

Figure 3: **Buckling pattern characteristics**. **a,** Schematic of the periodic unit cell used in the Bloch-Floquet analysis. Normalized critical wavenumber (obtained through Bloch-Floquet analysis) and the Fourier coefficient magnitudes of post-buckling patterns at multiple wavenumbers as the function of magnetization for the composites with various spacing ratios: **b,** $\xi = 0.36$, **c,** $\xi = 0.50$, and **d,** $\xi = 0.65$.

the Supplementary section S3.2.2).

To compare the results of Bloch-Floquet analysis with that of the post-buckling analysis, we evaluate the predominant wavenumbers in the post-buckling patterns. To this end, we apply the discrete Fourier transformation on the vertical displacement of inclusions forming the buckling pattern and obtain the Fourier coefficients f_k as the function of wavenumber k. The post-buckling configurations of inclusions in composites with $\xi = 0.36$, $\xi = 0.50$, and $\xi = 0.65$ are recorded at the compressive strains of $\varepsilon = 0.4$, $\varepsilon = 0.3$, and $\varepsilon = 0.17$, respectively.

Figure 3 show the results for both the analysis as the functions of magnetization level in the composites with spacing ratio $\xi = 0.36$ (b), $\xi = 0.50$ (c), and $\xi = 0.65$ (d). Note that the $y-$axis on the plots uses the normalized wavenumber $k^* = kw$ (w is the primitive unit cell width, see Fig. 1a), which relates to the number of inclusions in a wavelength as $N = 1/k^*$. The red curves show the critical wavenumber obtained through the Bloch-Floquet analysis and the blue circles correspond to the Fourier coefficients f_k obtained for the post-buckling patterns, where the diameter of circles is proportional to the magnitude of f_k.

The magnetic strength of inclusions can be explicitly partitioned into three groups on the basis of f_k values. First, in the composites with lower magnetization strength, we observe a single wavenumber with a significantly larger fourier coefficient that is associated with the mechanical wavy-pattern. For example, in the composites with $\xi = 0.65$ for $0 \lesssim M \lesssim 675$ kA/m, this wavenumber is $k^* = 0.20$, corresponding to the wavy-pattern with periodicity $N = 5$ (as shown in Fig. 2 left column). Similarly, at higher magnetization values, the f_k magnitude is considerably higher at one wavenumber; however, in this range it pertains to the two-level magnetic pattern with $k^* = 0.50$ (see right column in Fig. 2).

As previously discussed, the buckling pattern does not discretely switch from mechanical to magnetic with increase in the magnetic strength. Instead, there exist a range of magnetization values where the buckling patterns are distinctly different from both the mechanical and magnetic ones; we refer to this range as *transition region* (shaded in green color). In these region, we observe two types of buckling patterns: (i) with considerable magnitude of f_k at multiple k^* values, which implies a combination of multiple wavelengths in the buckling pattern (e.g., see the transition region in composites with $\xi = 0.36$ and $\xi = 0.50$); (ii) similar to mechanical and magnetic patterns, there is a significantly larger f_k magnitude at a single k^*, however, this wavenumber lies in between of mechanical and magnetic ones. For example, in the transition region of composites with $\xi = 0.65$, we obtain $k^* = 0.25$ corresponding to the periodic wavy-pattern shown in Fig. 2 central-bottom image. Moreover, we have analyzed how the buckling patterns in

the transition region geometrically correlates to the respective mechanical and magnetic patterns (see Supplementary Section S5).

We find that the critical wavenumbers, k^*_{cr}, determined via the Bloch-Floquet analysis also reveal the similar evolution from mechanical to magnetic instability patterns with increase in the magnetization. Initially, at smaller values of M, we observe a gradual increase in k^*_{cr}, which shows that the wavelength of the bifurcation eigenmodes decreases with increase in the magnetic strength of inclusions. This behavior can be attributed to the local repulsive interactions between the neighboring magnets that favor the rearrangement of inclusions into buckling patterns with smaller wavelengths. Moreover, the rate of change in the k^*_{cr} increases with the increase in M. Henceforth, at a certain threshold magnetization, we obtain a drastic increase in the critical wavenumber to $k^*_{cr} = 0.50$. Followed by that, the wavenumber remains constant – indicating the formation of two-level buckling patterns when the inclusions have higher magnetic strength than the threshold value (e.g., threshold magnetization value for $\xi = 0.50$ composite is 560 kA/m).

Considering the variation of critical wavenumber k^*_{cr}, we obtain two regions of magnetic strength: pre-threshold ($k^*_{cr} < 0.50$) and post-threshold ($k^*_{cr} = 0.50$). The results of both the analysis are in good agreement in the post-threshold or the magnetically-dominated region, i.e., the largest f_k value is obtained at $k^* = k^*_{cr} = 0.50$. However, in the pre-threshold region, the buckling patterns obtained via the post-buckling analysis do not show a continuous evolution, in contrast to what is observed for the bifurcation eigenmodes. As discussed previously, we observe sudden transitions in the instability patterns. This disparity highlights the key difference between the two methods used for predicting the instability development – Bloch-Floquet analysis considers an infinite number of unit cells, whereas the post-buckling simulations consider a finitely-sized specimen. Since the particulate composite is a discrete system, in the post-buckling regime, the inclusions can only rearrange into certain stable patterns to reduce geometric frustrations. Therefore, in the pre-threshold region, the buckling pattern is either a periodic wavy-pattern with wavelength containing an integer number of inclusions, or it is a superposition of multiple wavelengths. We note that a similar deviation in the results of two analysis is reported for the *purely* mechanical particulate composites [39].

Furthermore, we note that the transition region shifts to higher magnetization values with an increase in the spacing ratio. For example, in the composites with $\xi = 0.36$, the region lies approximately between $50 \lesssim M \lesssim 350$ kA/m, which shifts to $675 \lesssim M \lesssim 850$ kA/m at $\xi = 0.65$. This shift implies that it is comparatively easier to achieve two-level magnetic buckling patterns in a composite with far-placed inclusions, even when they are magnetically weak. However, when

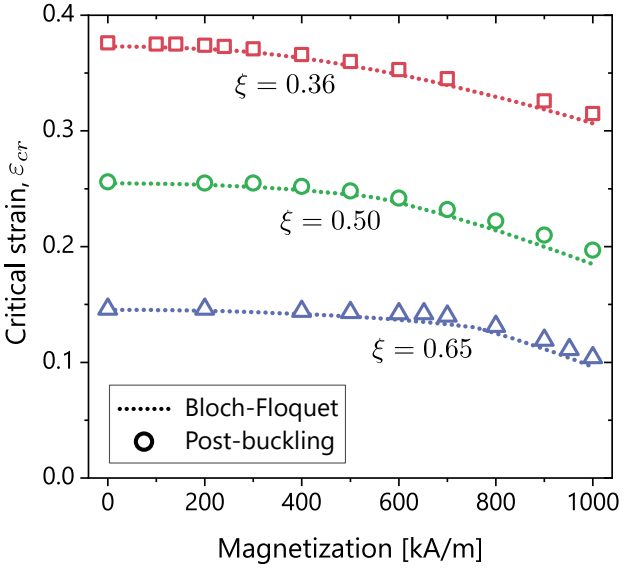

Figure 4: Dependence of critical strain ε_{cr} on the magnetization of inclusions.

the inclusion are initially closely-placed, the mechanical behavior dominates the formation of the post-buckling patterns.

Next, we analyze the dependence of instability onset on the magnetic strength of inclusions. In Fig. 4, we plot the critical strain ε_{cr} obtained through Bloch-Floquet analysis (dotted-curves) and post-buckling analysis (symbols) as the functions of magnetization. We observe that the composites develops instability at smaller strain levels (or ε_{cr} decreases) with an increase in magnetization. This destabilizing behavior is caused by the repulsive forces between the adjacent inclusions, leading to earlier onset of instabilities (also observed in experiments, see Fig. 1c). The critical strain values obtained through both the analysis are found to be in good agreement. We note that, unlike the sudden transitions observed in the buckling patterns in post-buckling simulations, ε_{cr} shows a gradual and monotonic decrease with an increase in magnetic strength.

Moreover, we examine the forces acting on the inclusion because of its neighbor at the point of instability. The study is performed on a simplified model consisting of magnetic inclusions connected via non-linear springs (for more details see Supplmentary Section S6). The total force acting on the inclusion is a sum of non-linear mechanical, $F_{mech}(\varepsilon)$, and magnetic, $F_{mag}(\varepsilon, M)$, forces. We find that there exists a *threshold* total force value that depends on the geometry of the composite, i.e., spacing ratio. Hence, the interplay of F_{mech} and F_{mag} determine the variation in critical strain with the change in magnetic strength of the inclusions.

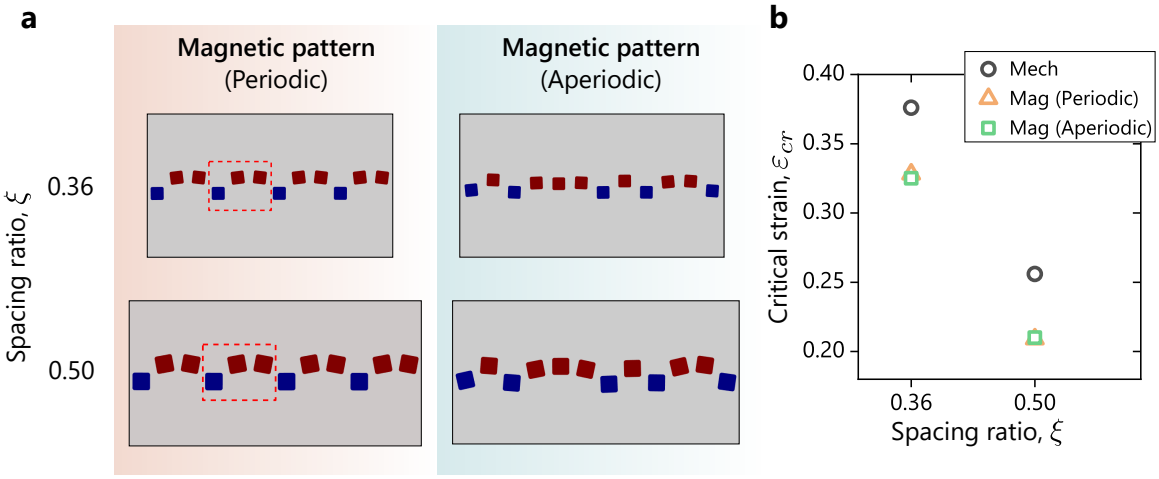

Figure 5: **Periodic and aperiodic reconfigurations.** **a**, Simulation images of particulate composites with spacing ratio $\xi = 0.36$ (top) and $\xi = 0.5$ (bottom). The results are shown for magnetic composites with periodic polarity pattern (left column) and aperiodic polarity pattern (right column) having magnetization $M = 900$ kA/m. **b**, Critical strain values for the composites considered in sub-figure a and their mechanical counterparts.

2.3 Programming buckling patterns and encoding information

Hitherto, we have investigated the pattern formations in composites possessing the same magnetic polarity arrangement – the adjacent inclusions repel each other. Next, we examine two distinct arrangements of magnetization orientations. The first polarity pattern is *periodic*, consisting of a repeating set of three inclusions with one negative magnetic polarity followed by two positives. The second one is an arbitrarily-chosen *aperiodic* polarity pattern. We consider the inclusions with sufficiently high magnetic strength, i.e., $M = 900$ kA/m, such that the formation of buckling patterns is dictated by the magnetic interactions. Figure 5 presents the numerical results for the instability development in these composites.

In magnetic composites with periodic polarity pattern, the magnets with negative polarity are surrounded by the pairs of positively polarized inclusions; hence, they are repelled by these pairs and vice-versa. On the other hand, among the inclusion pair with positive polarity, there is an attraction force. Guided by these magnetic interactions, in the buckling pattern, the negatively polarized magnets shift to form one row. All the positively polarized magnets rearrange in pairs to form the other row. Notably, identical buckling patterns are obtained in both the composites, regardless of their spacing ratios (deformation images are shown in the left column of Fig. 5a). Although the periodicity of these magnetic patterns is $N = 3$ (repeating periodic elements are

bounded by red-dashed rectangles), the arrangement of inclusions is noticeably different from that in mechanical composite with $\xi = 0.36$ (shown in the left column of Fig. 2). In particular, the magnetic pattern is a discrete two-level reconfiguration of inclusions, whereas the mechanical one is inherently a wave-like arrangement. We find that in the case of an aperiodic polarity pattern as well, the instability-induced shift in inclusions is governed by the resulting magnetic interactions. Consequently, the aperiodic buckling pattern emerges in the magnetic composites (Fig. 5a, right column). For both the magnetic patterns – periodic and aperiodic – the critical strain values are lower than their mechanical counterparts (Fig. 5b). Moreover, the critical strains for magnetic composites with a given spacing ratio are almost identical for periodic and aperiodic patterns, further indicating that the onset of instability is only dependent on the local interactions.

From the analysis thus far, two key features emanate from the magnetic buckling patterns. First, they are strictly guided by the (attraction/repulsion) magnetic forces between the inclusions, which leads to the formation of two-level microstructure patterns with inclusions of identical polarity lying in the same row. Second, these transformations are independent of the initial spacing ratio, ξ. Building upon these features, we can program any desired and deformation-activated microstructural transformations in the composite. In particular, the target two-level pattern can be achieved by encoding the magnetic bit scheme into the design of initially periodic composite. The magnetic bit scheme consists of pattern bits '0' and '1', physically denoting the two opposite orientations of magnets (Fig. 6a). The placement of bits in the scheme is planned according to the target microstructure pattern.

To showcase the complexity of achievable shapes, we consider the example of encoding the 'UW' pattern into the composite (Fig. 6b). The pattern is dissected into two-levels, such that it can be discretely represented by the arrangement of inclusions. Guided by the required positioning of the inclusions in the post-buckled state, we assign the magnetic pattern bits to each inclusion: zero for bottom row and one for top row. The magnetic bit scheme for the 'UW' pattern is obtained as '10010101'. We assess this scheme in an initially periodic particulate composite with spacing ratio $\xi = 0.5$. In the composite, the magnetic inclusions are embedded with polarity pattern that follows the aforementioned magnetic bit scheme. Under compressive strain greater than the critical value, the inclusions depart from their initial periodic arrangement and indeed reconfigure to form the target 'UW' pattern. The experimental and simulation deformation images are shown at the strain-level $\varepsilon = 0.35$ in Fig. 6b (also see Supplementary Video 1).

Finally, we present the encoding of binary information, specifically, Morse code in our architected material, and analyze the consequent instability-induced transformations. Morse code is a

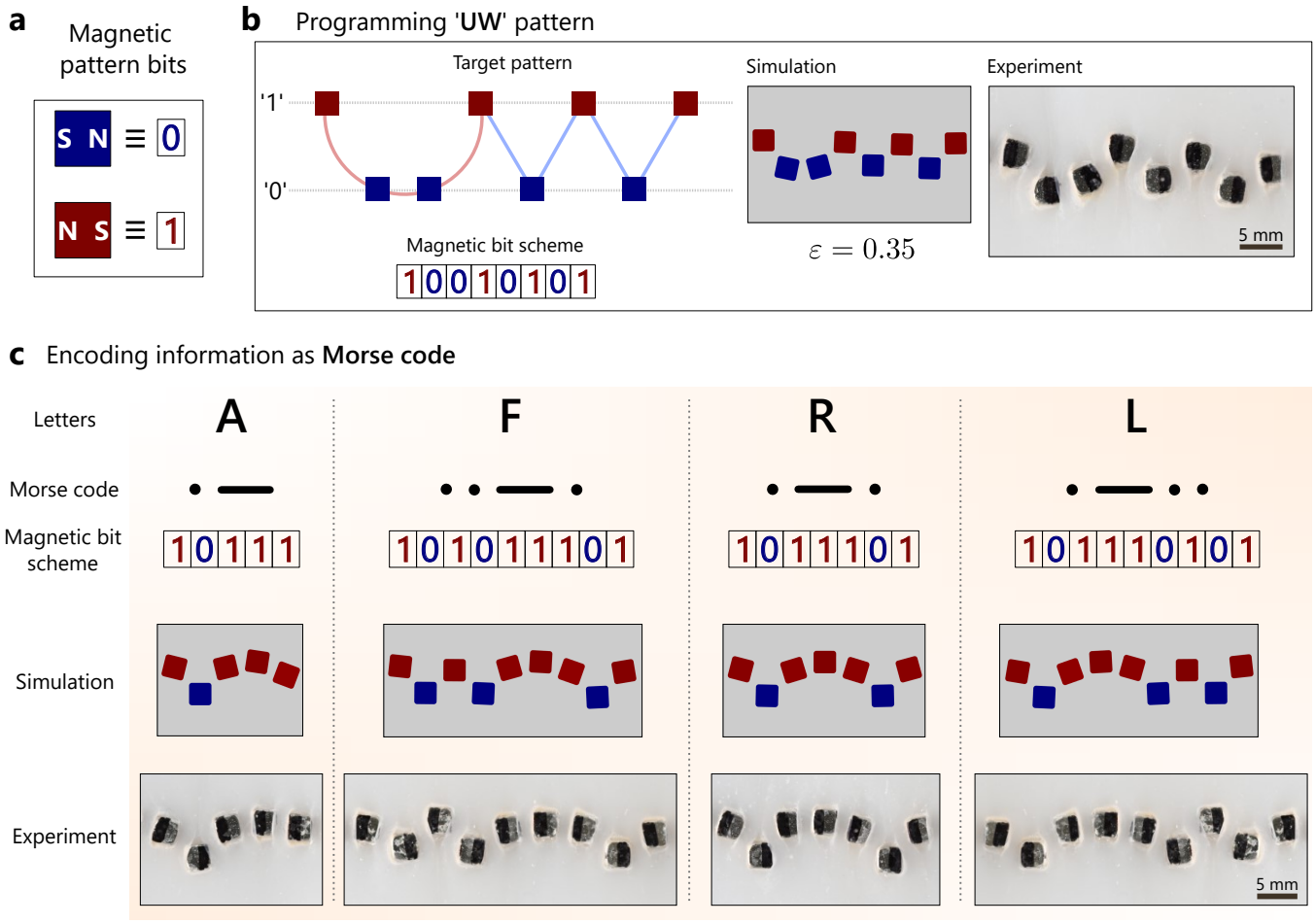

Figure 6: **Programming instability patterns and encoding information.** **a**, Physical definition of the magnetic pattern bits that constitutes the magnetic bit scheme. **b**, Programming 'UW' pattern. Discretization of 'UW' pattern into two levels and the analogous bit scheme. The corresponding simulation and experimental images are shown on the right. **c**, Encoding information as Morse code. From top to bottom: the letters, their Morse code, magnetic bit schemes, the simulation results, and the experimental deformation images. The results are shown for the composites with spacing ratio $\xi = 0.5$ subjected to a compressive strain of $\varepsilon = 0.35$.

method to encode text in the form of dots and dashes. In terms of ON-OFF keying, in a single letter, a dot represents one ON signal, whereas a dash denotes a series of three ON signals. The space in the Morse code is the equivalent of one OFF. To encode Morse code in our composites, we represent ON and OFF signals as '1' and '0', respectively.

As illustrative examples, we encode the Morse code of four letters, 'A', 'F', 'R', and 'L'. The magnetic bit scheme, that is fed into the design of the composite, is directly derived from the Morse code in the binary form (as shown in the 'Bit scheme' row in Fig. 6c). Each letter gives rise to distinct deformation modes in the post-instability regime. In particular, following the input polarity arrangement, the inclusions rearrange into distinct binary patterns. These patterns are identically revealed by our experiments and finite element simulations (the bottom two rows in Fig. 6c show the deformation images at strain $\varepsilon = 0.35$). The stored binary information can be decoded from the relative positioning of the inclusions. Therefore, in the present system, the information can be encoded in the magnetic form and read out via the applied mechanical deformation in the form of buckling patterns.

We note that in the magnetic bit scheme-guided reconfiguration of inclusions, it is not necessary that the inclusions with negative polarity always shift to form the bottom row. In an ideal setting, an opposite pattern, constituting negative polarity inclusions in the top row and positive ones in the bottom row, is equally probable. However, unique information bits can be assigned to the top and bottom position by using an extra inclusion as a reference, similar to setting a ground-level bit in electrical signals (more details are provided in Supplementary Sec. S7 and Fig. S14b). Moreover, the presence of initial geometric or material defects can potentially affect the buckling patterns. The extent of perturbations, however, can be reduced by producing magnetic composites through various additive manufacturing techniques across length scales [40–49]. Additionally, employment of these techniques to fabricate the magneto-elastic materials can automate and simplify the manufacturing process. On the other hand, these imperfections can be capitalized to enrich the admissible range of buckling patterns [50].

3 Conclusion

Our strategy enables the development of reconfigurable architected materials with magnetically-programmed structural transformations. The pixel-level programmability of the deformation modes is achieved by the local magnetic interactions between the inclusions, thereby, guiding their rearrangement in the post-buckling state. This approach can be readily implemented into the designs of other material-based systems. The strategy presented here opens the door to a

broad range of applications in which the local shape-tunability of the architecture is instrumental. We have selected the alphabet and Morse code examples to demonstrate the rich tuning capability of our magneto-mechanical system in encoding meaningful abstractions. Although of very low bit density compared to conventional memory devices, this information encoding has the distinct advantage of direct coupling with its mechanical environment to activate (or deactivate) the message. This feature is particularly relevant for sensing applications where threshold detection of applied mechanical strain or magnetic field is the target of interest. We also anticipate the pre-programmed shape morphing, for example, can be used to incorporate complex actuation and control capabilities into the soft robots [51]. Moreover, in soft particulate composites, the positioning of inclusions can be used to control the surface texture [52], thereby tuning their drag, friction, and wettability. Notably, by expanding beyond just two magnetization orientations in our design, we can further enrich the range of admissible buckling patterns with an increased control over the local interaction between the inclusions. Lastly, we envision the design of a re-programmable architected material in which the magnetic polarity of the inclusions can be reoriented through an external magnetic field.

Acknowledgments

The authors thank the support from the University of Wisconsin–Madison with funding from the Wisconsin Alumni Research Foundation. The authors acknowledge the support of the Air Force Office of Scientific Research (AFOSR 17RXCOR435), the European Office of Aerospace Research and Development (EOARD 19IOE010), and the Air Force Research Laboratory Materials and Manufacturing Directorate.

References

[1] M. Frey, G. Biffi, M. Adobes-Vidal, M. Zirkelbach, Y. Wang, K. Tu, A. M. Hirt, K. Masania, I. Burgert, T. Keplinger, Tunable wood by reversible interlocking and bioinspired mechanical gradients, Advanced science 6 (10) (2019) 1802190.

[2] M. Kamperman, A. Synytska, Switchable adhesion by chemical functionality and topography, Journal of Materials Chemistry 22 (37) (2012) 19390–19401.

[3] M. Zhang, H. Shahsavan, Y. Guo, A. Pena-Francesch, Y. Zhang, M. Sitti, Liquid-crystal-

elastomer-actuated reconfigurable microscale kirigami metastructures, Advanced Materials 33 (25) (2021) 2008605.

[4] J. Zhu, M. Dexheimer, H. Cheng, Reconfigurable systems for multifunctional electronics, npj Flexible Electronics 1 (1) (2017) 1–13.

[5] Z. Wang, L. Jing, K. Yao, Y. Yang, B. Zheng, C. M. Soukoulis, H. Chen, Y. Liu, Origami-based reconfigurable metamaterials for tunable chirality, Advanced materials 29 (27) (2017) 1700412.

[6] R. M. Erb, J. S. Sander, R. Grisch, A. R. Studart, Self-shaping composites with programmable bioinspired microstructures, Nature communications 4 (1) (2013) 1–8.

[7] Y. Zhang, M. Velay-Lizancos, D. Restrepo, N. D. Mankame, P. D. Zavattieri, Architected material analogs for shape memory alloys, Matter 4 (6) (2021) 1990–2012.

[8] T. Frenzel, M. Kadic, M. Wegener, Three-dimensional mechanical metamaterials with a twist, Science 358 (6366) (2017) 1072–1074.

[9] T. Chen, O. R. Bilal, K. Shea, C. Daraio, Harnessing bistability for directional propulsion of soft, untethered robots, Proceedings of the National Academy of Sciences 115 (22) (2018) 5698–5702.

[10] F. Bobbert, S. Janbaz, A. Zadpoor, Towards deployable meta-implants, Journal of Materials Chemistry B 6 (21) (2018) 3449–3455.

[11] Y. Kim, X. Zhao, Magnetic soft materials and robots, Chemical reviews 122 (5) (2022) 5317–5364.

[12] S. Palagi, A. G. Mark, S. Y. Reigh, K. Melde, T. Qiu, H. Zeng, C. Parmeggiani, D. Martella, A. Sanchez-Castillo, N. Kapernaum, et al., Structured light enables biomimetic swimming and versatile locomotion of photoresponsive soft microrobots, Nature materials 15 (6) (2016) 647–653.

[13] R. Geryak, V. V. Tsukruk, Reconfigurable and actuating structures from soft materials, Soft matter 10 (9) (2014) 1246–1263.

[14] M. Behl, A. Lendlein, Actively moving polymers, Soft Matter 3 (1) (2007) 58–67.

[15] A. Pal, M. Sitti, Programmable mechanical devices through magnetically tunable bistable elements, Proceedings of the National Academy of Sciences 120 (15) (2023) e2212489120.

[16] X. Xia, C. M. Spadaccini, J. R. Greer, Responsive materials architected in space and time, Nature Reviews Materials 7 (9) (2022) 683–701.

[17] T. Mullin, S. Deschanel, K. Bertoldi, M. C. Boyce, Pattern transformation triggered by deformation, Phys. Rev. Lett. 99 (8) (2007) 84301. doi:10.1103/PhysRevLett.99.084301.

[18] D. M. Kochmann, K. Bertoldi, Exploiting microstructural instabilities in solids and structures: from metamaterials to structural transitions, Applied mechanics reviews 69 (5) (2017) 050801.

[19] Y. Jiang, L. M. Korpas, J. R. Raney, Bifurcation-based embodied logic and autonomous actuation, Nature communications 10 (1) (2019) 1–10.

[20] K. Bertoldi, P. M. Reis, S. Willshaw, T. Mullin, Negative poisson's ratio behavior induced by an elastic instability, Advanced materials 22 (3) (2010) 361–366.

[21] P. Wang, F. Casadei, S. Shan, J. C. Weaver, K. Bertoldi, Harnessing Buckling to Design Tunable Locally Resonant Acoustic Metamaterials, Phys. Rev. Lett. 113 (1) (2014) 014301. doi:10.1103/PhysRevLett.113.014301.

[22] D. Krishnan, H. Johnson, Optical properties of two-dimensional polymer photonic crystals after deformation-induced pattern transformations, J. Mech. Phys. Solids 57 (9) (2009) 1500–1513.

[23] J. Li, J. Shim, J. Deng, J. T. Overvelde, X. Zhu, K. Bertoldi, S. Yang, Switching periodic membranes via pattern transformation and shape memory effect, Soft Matter 8 (40) (2012) 10322–10328.

[24] S. H. Kang, S. Shan, A. Košmrlj, W. L. Noorduin, S. Shian, J. C. Weaver, D. R. Clarke, K. Bertoldi, Complex ordered patterns in mechanical instability induced geometrically frustrated triangular cellular structures, Physical review letters 112 (9) (2014) 098701.

[25] T. Frenzel, C. Findeisen, M. Kadic, P. Gumbsch, M. Wegener, Tailored buckling microlattices as reusable light-weight shock absorbers, Advanced Materials 28 (28) (2016) 5865–5870.

[26] H. Cho, J. C. Weaver, E. Pöselt, P. J. in't Veld, M. C. Boyce, G. C. Rutledge, Engineering the mechanics of heterogeneous soft crystals, Advanced Functional Materials 26 (38) (2016) 6938–6949.

[27] N. Triantafyllidis, B. N. Maker, On the comparison between microscopic and macroscopic instability mechanisms in a class of fiber-reinforced composites, J. Appl. Mech., Trans. ASME 52 (1985) 794–800.

[28] J. Li, T. D. Pallicity, V. Slesarenko, A. Goshkoderia, S. Rudykh, Domain formations and pattern transitions via instabilities in soft heterogeneous materials, Advanced Materials 31 (14) (2019) 1807309.

[29] C. Jiang, S. Singamaneni, E. Merrick, V. V. Tsukruk, Complex buckling instability patterns of nanomembranes with encapsulated gold nanoparticle arrays, Nano letters 6 (10) (2006) 2254–2259.

[30] W. Hu, G. Z. Lum, M. Mastrangeli, M. Sitti, Small-scale soft-bodied robot with multimodal locomotion, Nature 554 (7690) (2018) 81–85.

[31] R. F. Shepherd, F. Ilievski, W. Choi, S. A. Morin, A. A. Stokes, A. D. Mazzeo, X. Chen, M. Wang, G. M. Whitesides, Multigait soft robot, Proceedings of the national academy of sciences 108 (51) (2011) 20400–20403.

[32] A. Chortos, J. Liu, Z. Bao, Pursuing prosthetic electronic skin, Nature materials 15 (9) (2016) 937–950.

[33] W. Zeng, L. Shu, Q. Li, S. Chen, F. Wang, X.-M. Tao, Fiber-based wearable electronics: a review of materials, fabrication, devices, and applications, Advanced materials 26 (31) (2014) 5310–5336.

[34] T. Y. K. Ho, A. Nirmal, M. R. Kulkarni, D. Accoto, N. Mathews, Soft actuator materials for electrically driven haptic interfaces, Advanced Intelligent Systems 4 (2) (2022) 2100061.

[35] H. Fu, K. Nan, W. Bai, W. Huang, K. Bai, L. Lu, C. Zhou, Y. Liu, F. Liu, J. Wang, et al., Morphable 3d mesostructures and microelectronic devices by multistable buckling mechanics, Nature materials 17 (3) (2018) 268–276.

[36] M. Amjadi, K.-U. Kyung, I. Park, M. Sitti, Stretchable, skin-mountable, and wearable strain sensors and their potential applications: a review, Advanced Functional Materials 26 (11) (2016) 1678–1698.

[37] H. Yasuda, P. R. Buskohl, A. Gillman, T. D. Murphey, S. Stepney, R. A. Vaia, J. R. Raney, Mechanical computing, Nature 598 (7879) (2021) 39–48.

[38] C. El Helou, P. R. Buskohl, C. E. Tabor, R. L. Harne, Digital logic gates in soft, conductive mechanical metamaterials, Nature communications 12 (1) (2021) 1–8.

[39] D. Chen, Y. Xiang, N. Arora, Q. Yao, J. Li, S. Rudykh, Post-buckling development in soft particulate composites, Composite Structures 322 (2023) 117337.

[40] Y. Kim, H. Yuk, R. Zhao, S. A. Chester, X. Zhao, Printing ferromagnetic domains for untethered fast-transforming soft materials, Nature 558 (2018) 274–279.

[41] Y. Zhang, Q. Wang, S. Yi, Z. Lin, C. Wang, Z. Chen, L. Jiang, 4d printing of magnetoactive soft materials for on-demand magnetic actuation transformation, ACS Applied Materials & Interfaces 13 (3) (2021) 4174–4184.

[42] X. Cao, S. Xuan, S. Sun, Z. Xu, J. Li, X. Gong, 3d printing magnetic actuators for biomimetic applications, ACS applied materials & interfaces 13 (25) (2021) 30127–30136.

[43] Z. Wang, Y. Wu, D. Wu, D. Sun, L. Lin, Soft magnetic composites for highly deformable actuators by four-dimensional electrohydrodynamic printing, Composites Part B: Engineering 231 (2022) 109596.

[44] S. Lantean, G. Barrera, C. F. Pirri, P. Tiberto, M. Sangermano, I. Roppolo, G. Rizza, 3d printing of magnetoresponsive polymeric materials with tunable mechanical and magnetic properties by digital light processing, Advanced Materials Technologies 4 (11) (2019) 1900505.

[45] S. Sundaram, M. Skouras, D. S. Kim, L. van den Heuvel, W. Matusik, Topology optimization and 3d printing of multimaterial magnetic actuators and displays, Science advances 5 (7) (2019) eaaw1160.

[46] S. Wu, C. M. Hamel, Q. Ze, F. Yang, H. J. Qi, R. Zhao, Evolutionary algorithm-guided voxel-encoding printing of functional hard-magnetic soft active materials, Advanced Intelligent Systems 2 (8) (2020) 2000060.

[47] Y. Dong, S. Wang, Y. Ke, L. Ding, X. Zeng, S. Magdassi, Y. Long, 4d printed hydrogels: fabrication, materials, and applications, Advanced Materials Technologies 5 (6) (2020) 2000034.

[48] M. L. Lopez-Donaire, G. de Aranda-Izuzquiza, S. Garzon-Hernandez, J. Crespo-Miguel, M. Fernandez-de la Torre, D. Velasco, D. Garcia-Gonzalez, Computationally guided diw technology to enable robust printing of inks with evolving rheological properties, Advanced Materials Technologies 8 (3) (2023) 2201707.

[49] L. Lu, P. Guo, Y. Pan, Magnetic-field-assisted projection stereolithography for three-dimensional printing of smart structures, Journal of Manufacturing Science and Engineering 139 (7) (2017).

[50] L. Liu, P. Kamm, F. García-Moreno, J. Banhart, D. Pasini, Elastic and failure response of imperfect three-dimensional metallic lattices: the role of geometric defects induced by selective laser melting, Journal of the Mechanics and Physics of Solids 107 (2017) 160–184.

[51] A. Pal, V. Restrepo, D. Goswami, R. V. Martinez, Exploiting mechanical instabilities in soft robotics: Control, sensing, and actuation, Advanced Materials 33 (19) (2021) 2006939.

[52] M. Guttag, M. C. Boyce, Locally and dynamically controllable surface topography through the use of particle-enhanced soft composites, Advanced Functional Materials 25 (24) (2015) 3641–3647.